WEP Warwick Evans Publishing

International Journal of Materials Science and Technology Studies

ISSN: 3006-7693 (Print), ISSN: 3006-3744 (Online) | Volume 1, Number 1, Year 2024
DOI: https://doi.org/10.62051//ijmsts.v1n1.10
Journal homepage: https://wepub.org/index.php/IJMSTS/index

Electrochemical properties of spinel $LiMn_{1.92-x}Cu_{0.08}Ni_xO_4$ cathode material prepared by a solution combustion method

Yonggen Li [1], Jianqiang Zhang [1], Yin Liu [2], Wei Jiang [1], Mei Chen [1]

[1] School of Biology and Chemistry, Pu'er University, Pu'er, Yunnan, 665000, China

[2] Yunnan Kunming Branch, Hydrology and Water Resources Bureau, Kunming, Yunnan, 65005, China

ABSTRACT

A series of Ni-Cu co-doped spinel $LiMn_{1.92-x}Cu_{0.08}Ni_xO_4$ cathode materials were successfully synthesized by a solution combustion method. X-ray diffraction (XRD) spectra showed that all the as-prepared $LiMn_{1.92-x}Cu_{0.08}Ni_xO_4$ samples belong to spinel $LiMn_2O_4$ structure without any impurity phase. Scanning electron microscopy (SEM) showed that the particle size of the samples decreased with the increase of Ni-doping amount, and the crystallinity increased gradually. The galvanostatic charge/discharge tests results showed that the $LiMn_{1.86}Cu_{0.08}Ni_{0.06}O_4$ sample shows excellent rate performance and cyclic stability. At room temperature and 1 C, the initial discharge specific capacity of $LiMn_{1.86}Cu_{0.08}Ni_{0.06}O_4$ was 103.4 mAh g^{-1}, and the capacity retention rate of 67.80% was obtained after 1000 cycles, which was higher than 49.60% of $LiMn_2O_4$. Even at high current densities of 5 C and 10 C, the good capacity retention rates of 73.55% and 67.29% for $LiMn_{1.86}Cu_{0.08}Ni_{0.06}O_4$ sample were obtained after 1000 cycles, respectively.

KEYWORDS

Spinel lithium manganate; Solution combustion method; Ni-doping; Cathode material.

1. INTRODUCTION

Spinel lithium manganate (LiMn [1] O_4 . When spinel $LiMn_2O_4$ is used as the cathode material of lithium ion battery, it has the characteristics of low price, high theoretical discharge specific capacity (148.2 mAh g^{-1}, high energy density (~125 Wh kg^{-1}, high working voltage (~3.6V), good safety performance, low self discharge rate (6-9%/month) and environmental friendliness Aerospace and other fields have achieved rapid development [2, 3]. However, in the actual charging and discharging process, the specific discharge capacity of spinel $LiMn_2O_4$ is only about 120.0 mAh g^{-1}, and the cycle stability is poor, especially at high temperature (≥ 55°C) and high magnification, the attenuation is particularly rapid [4]. The main reasons are: (1) the disproportionation reaction of Mn^{3+} dissolved in the electrolyte generates soluble Mn^{2+} and strongly oxidizing Mn^{4+} [5, 6]; (2) Spinel structure distortion caused by Jahn Teller effect [7, 8]; (3) Electrolyte is easy to decompose under high pressure (≥ 4.5V), or react with trace H_2O in the system, and finally generate incompletely electrochemically active λ- MnO_2 [9]; (4) under high temperature conditions, oxygen defects are prone to occur, forming anoxic $LiMn_2O_4$. The average valence of Mn decreases, which aggravates the Jahn Teller effect [10].

At present, the methods of modifying spinel $LiMn_2O_4$ cathode materials mainly include element doping, surface coating and process optimization, forming a special morphology that is more conducive to Li^+ diffusion or reduces the dissolution of Mn^{3+}, to improve the cycle stability and magnification of the entire battery [11]. Among the three modification methods, element doping is widely used, and the improvement effect is obvious. Nie Wei et al. [12] doped $LiNi_{0.5}Mn_{1.5}O_4$

cathode material with alkaline earth metals Mg^{2+}, Ca^{2+} and Ba^{2+}. The results show that $LiNi_{0.5}Mn_{1.5}O_4$ sintered at 1 C and 2 75~5. The capacity retention rates of $LiM_{0.1}Ni_{0.4}Mn_{1.5}O_4$ (M=Mg, Ca and Ba) after 100 charge discharge cycles were 78.3% and 83.6% respectively, while the capacity retention rates of modified $LiM_{0.1}Ni_{0.4}Mn_{1.5}O_4$ (M=Mg, Ca and Ba) after primary sintering were 90.1%, 96.0% and 96.2% respectively, and the capacity retention rates of secondary sintering were 90.6%, 96.8% and 89.5% respectively. A. Iqbal et al. [13] prepared $LiNi_xCu_yMn_{2-x-y}O_4$ x=y=0.01-0.05) lithium ion cathode material by citric acid assisted sol-gel method. When conducting constant current charge and discharge tests at a current density of 0.3 C and a working voltage of 3.0~4.8V, $LiNi_{0.01}Cu_{0.01}Mn_{1.98}O_4$ samples showed the maximum initial discharge specific capacity of 113 mAh g^{-1}, The maximum capacity retention rate of 88% was obtained after 100 charge discharge cycles. Based on the above research, this paper discussed the influence of Ni^{2+} doping on the microstructure and morphology, electrochemical and kinetic properties of $LiMn_{1.92}Cu_{0.08}O_4$.

2. EXPERIMENTAL METHODS

2.1. Preparation of $LiMn_{1.92-x}Cu_{0.08}Ni_xO_4$

$LiNO_3$ AR), Mn $(CH_3COO)_2 \cdot 4H_2O$ (AR), Cu $(NO_3)_2$ $3H_2O$ (AR) and Ni $(CH_3COO)_2 \cdot 4H_2O$ (AR) are used as raw materials, and Li: Mn: Cu: Ni=1:1.92-x: 0.08: x (x=0, 0.02, 0.04, 0.06 ,0.08 and 0.10 are used for short LMCNO-0.08, LMCNO-0.08-0.02, LMCNO-0.08-0.04, LMCNO-0.08-0.06, LMCNO-0.08-0.08 and LMCNO-0.08-0.10) After accurate weighing, put it into a 300 mL porcelain crucible, and add 3.5 mL HNO_3 (AR) as solvent and auxiliary reducing agent. Place the top crucible with raw materials in a 720W household microwave oven, preheat and dissolve it for 30s to form a solution, shake it gently by hand to mix it evenly. Continue heating and burning in 720W microwave for 5 min to obtain black and fluffy products. The product is ground into powder, and calcined in muffle furnace with preset temperature of 600℃ for 4 hours to obtain the target product.

2.2. Assembly of CR2030 battery

The prepared $LiMn_{1.92-x}Cu_{0.08}Ni_xO_4$ active substance, acetylene black and polyvinylidene fluoride (PVDF) are accurately weighed according to the mass ratio of 80:10:10, and then put into a ball milling tank, add an appropriate amount of N-methyl-2-pyrrolidone as a dispersant, and ball mill on a planetary ball mill for 30 minutes to obtain mixed slurry. Evenly coat the mixed slurry on the aluminum foil, dry it, and cut it into a positive material disc with a diameter of 16 mm. The calculation formula of the mass load (M_L, unit: mg/cm^2) of the active substance in the electrode is as follows:

$$M_L = [(M_T - M_A)*0.8]/[\pi*(16/2)^2*10^{-2}] \quad (1)$$

M_T and M_A in the formula respectively represent the total mass of the electrode plate and the mass of the aluminum foil. In the high-purity Ar glove box (super1220/750), a CR2032 button lithium ion battery was assembled with a lithium metal sheet as the negative electrode, $LiPF_6$ as the electrolyte, and polypropylene microporous membrane as the diaphragm.

2.3. Structural Characterization and Performance Testing

The phase of the sample powder was analyzed by X-ray diffractometer (XRD, D8 ADVANCE, Bruker Company), scanning range 2 θ 10°~70°. Scanning electron microscope (SEM, NOVANANOSEM 450, FEI Company of the United States) was used to analyze the microscopic particle size and morphology of the sample powder; LAND constant current test system (Wuhan Jinnuo Electronics Co., Ltd.) was used to test the battery power in the voltage range of 3.0~4.5V (1 C=148.0 mAh g^{-1}); The electrochemical workstation (CHI 660E model, Shanghai Chenhua

Instrument Co., Ltd.) was used to conduct cyclic voltammetry (CV) and electrochemical impedance (EIS, scanning frequency 0.1 Hz~100 kHz) tests in the voltage range of 3.6~4.5V.

3. RESULTS AND DISCUSSION

3.1. Characterization and analysis of macroscopic morphology

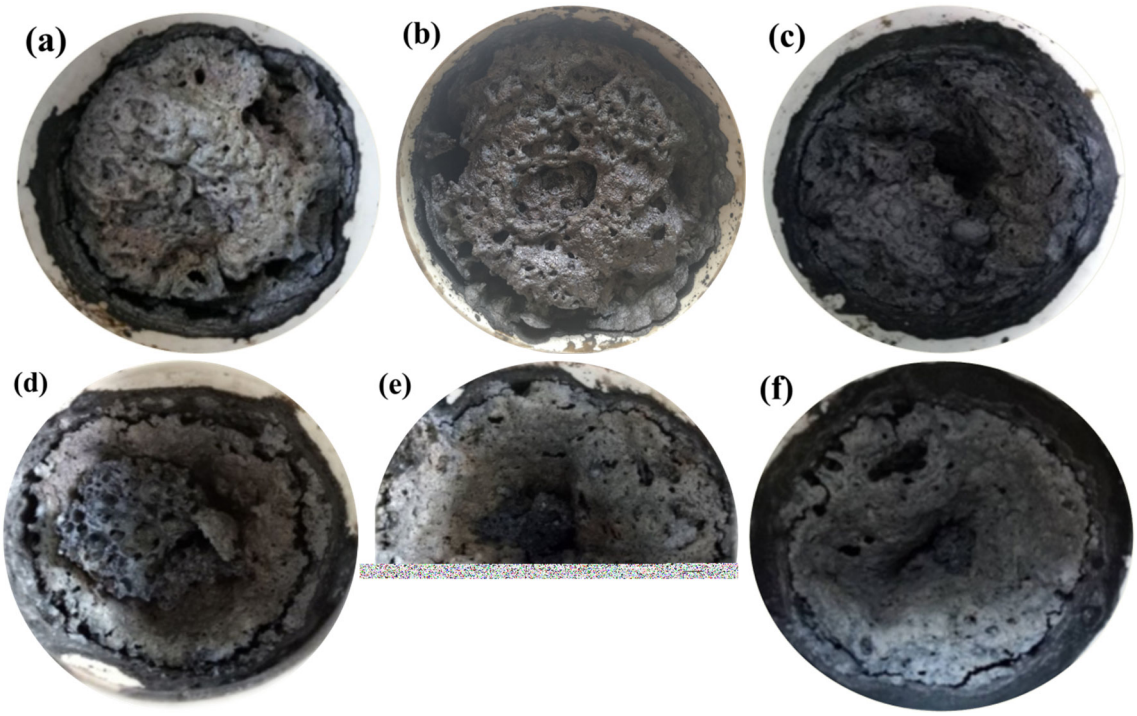

Figure 1. Macroscopic view of $LiMn_{1.92-x}Cu_{0.08}Ni_xO_4$: (a) x=0; (b) x=0.02; (c) x=0.04; (d) x=0.06; (e) x=0.08; (f) x=0.10;

Figure 1 shows the macroscopic morphology of the products synthesized after the mixed solution of various raw materials was burned for 5min under the power of 720W household frequency conversion microwave. It can be seen that the products obtained show black fluffy porous morphology. The fluffy structure starts from the bottom of the crucible and grows outward. With the increase of nickel acetate content, the "degree of consolidation" of the products has increased to a certain extent, resulting in the phenomenon of "hollow" collapse. This is because when the solution is heated in a closed microwave oven, the microwave energy mainly starts from the bottom tray in the oven, penetrates the sample instantly, reaches the self ignition point of the material itself, and heats the material directly from inside. During the combustion process, a certain amount of CO_2 is also generated. Secondly, because the concentrated nitric acid added in the system decomposes in the combustion process, generating gases such as NO_2 and O_2, which expand the volume of the product, it can be found that yellow thick smoke overflows during the combustion process, and the generation of O_2 can play the role of combustion supporting agent for combustion reaction.

3.2. Scanning electron microscope (SEM) analysis

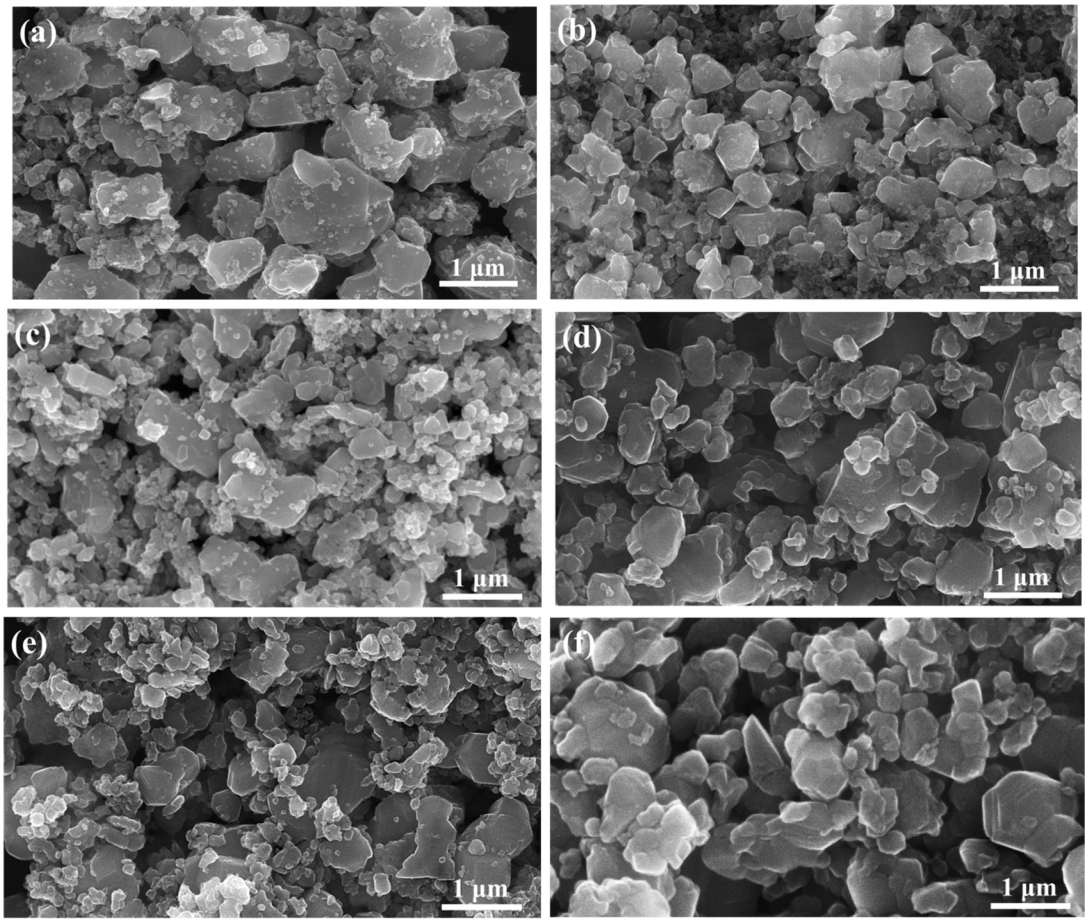

Figure 2. SEM diagram of $LiMn_{1.92-x}Cu_{0.08}Ni_xO_4$: (a) x=0; (b) x=0.02; (c) x=0.04; (d) x=0.06; (e) x=0.08; (f) x=0.10;

Figure 2 shows the SEM diagram of $LiMn_{1.92-x}Cu_{0.08}Ni_xO_4$ ($0 \leq x \leq 0.1$) sample. It can be seen from the figure that the particle size of the sample tends to decrease with the increase of Ni^{2+} doping amount, indicating that the doping of Ni^{2+} helps to promote the nucleation rate of particles, and the crystallinity increases [18]. This result is consistent with the analysis results obtained by XRD, which is due to the smaller ion radius of Ni than Mn. The small particle size can effectively shorten the length of Li^+ diffusion channel, facilitate the migration and diffusion of Li^+ in the spinel lattice, increase the reaction rate and diffusion kinetics, and thus significantly improve the electrochemical performance [19, 20].

3.3. Cycle performance test

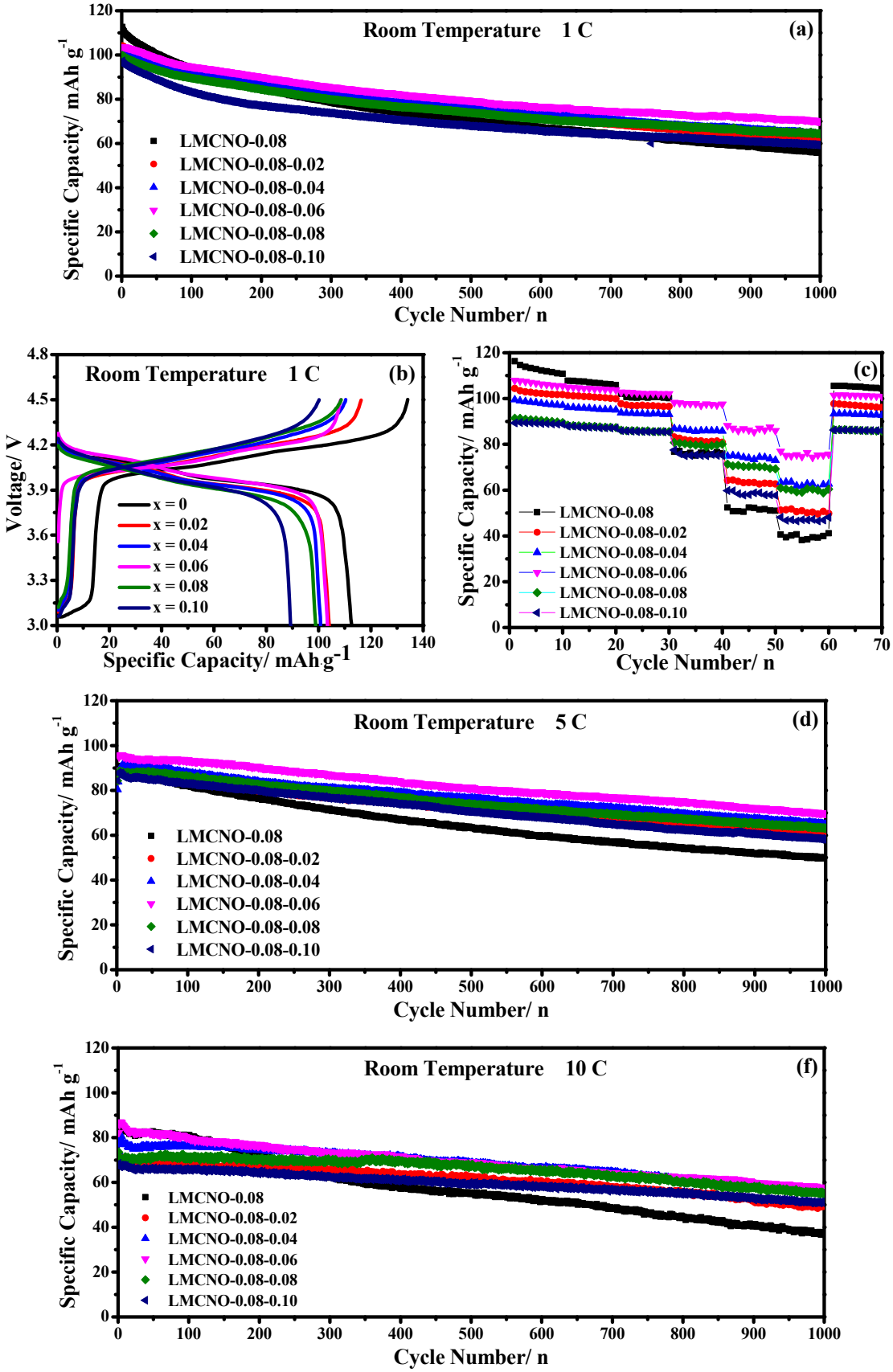

Figure 3. Cyclic performance diagram (a) and first charge discharge curve (b) of $LiMn_{1.92-x}Cu_{0.08}Ni_xO_4$ at room temperature 1 C; Multiplication performance diagram (c); Cyclic performance diagram at 5 C and 10 C (d), (e)

Table 1. Discharge specific capacity and capacity retention rate of $LiMn_{1.92-x}Cu_{0.08}Ni_xO_4$ at room temperature 1 C

sample	Discharge specific capacity (mAh g^{-1})		Capacity retention (%)
	For the first time	1000 times	
$LiMn_{1.92}Cu_{0.08}O_4$	112.7	55.9	49.60
$LiMn_{1.90}Cu_{0.08}Ni_{0.02}O_4$	104.1	62.0	59.16
$LiMn_{1.88}Cu_{0.08}Ni_{0.04}O_4$	100.8	64.3	63.79
$LiMn_{1.86}Cu_{0.08}Ni_{0.06}O_4$	103.4	70.1	67.80
$LiMn_{1.84}Cu_{0.08}Ni_{0.08}O_4$	99.9	64.3	64.36
$LiMn_{1.82}Cu_{0.08}Ni_{0.10}O_4$	97.3	59.4	61.05

Figure 3a shows the cyclic performance curve of $LiMn_{1.92-x}Cu_{0.08}Ni_xO_4$ ($0 \le x \le 0.1$) sample at room temperature of 1 C. The corresponding first charge discharge curve is shown in Figure 3b. It can be seen from Figure 3b that the first charge discharge curves of all synthetic products show two charge discharge plaorms at 3.9/4.1 V and 4.1/4.2 V, which is shown as the two-step reversible reaction of Li(81)in the charge discharge process, namely:

$$LiMn_2O_4 = Li_{0.5}Mn_2O_4 + 0.5\ Li^+ + 0.5\ e^- \quad (2)$$

$$Li_{0.5}Mn_2O_4 = 2\ \lambda\text{-}MnO_2 + 0.5\ Li^+ + 0.5\ e^- \quad (3)$$

It shows that the doping of Ni^{2+} does not change the de embedding mechanism [21] of Li^+ during the cycle. Table 1 shows that the specific capacity of the first discharge of the product $LiMn_{1.92-x}Cu_{0.08}Ni_xO_4$ ($0 \le x \le 0.1$) at x=0, 0.02, 0.04, 0.06, 0.08 and 0.10 is 112.7, 104.1, 100.8, 103.4, 99.9 and 97.3 mAh g^{-1} respectively. It can be seen that the specific capacity of the first discharge tends to decrease with the increase of Ni^{2+} doping, because Ni^{2+} replaces part of the active ion Mn^{3+} [22]. However, after 1000 cycles, it first increased and then decreased, reaching the maximum value of 67.80% when x=0.06, indicating a good Li^+ de embedding reversibility.

Figure 3c shows the magnification performance of $LiMn_{1.92-x}Cu_{0.08}Ni_xO_4$ ($0 \le x \le 0.1$) samples at different current densities (0.5, 1, 2, 5, 8, 10 and 0.5 C). It can be seen from the figure that due to the enhanced battery polarization under high current, the migration of Li^+ in the material is blocked, and the utilization rate of active substance decreases [23]. The discharge specific capacity of all products decreases with the increase of discharge magnification. The sample LMCNO-0.08 emits a high specific capacity of 116.3 mAh g^{-1} at 0.5 C. However, with the increase of current, the capacity has a sharp decline. When the current is 10 C, the discharge specific capacity is only 40.6 mAh g^{-1}, and its rate performance is extremely unstable. However, the sample LMCNO-0.08-0.06 has no attenuation at low magnification, and the maximum specific capacity of 88.2 mAh g^{-1} and 76.9 mAh g^{-1} can be released even when the high current is 8 C and 10 C, respectively.

Figure 3d and Figure 3e are the cyclic curves of $LiMn_{1.92-x}Cu_{0.08}Ni_xO_4$ ($0 \le x \le 0.1$) samples at room temperature 5 C and 10 C, respectively. It can be seen from Figure 3d and Figure 3e that, compared with the discharge specific capacity at room temperature of 1 C, the discharge specific capacity at 5 C and 10 C shows an obvious decreasing trend, which is due to the enhanced polarization of the battery under high current. This result is consistent with the results of the magnification performance analysis in Figure 3c. The cycle performance of LMCNO-0.08-0.06 sample at 5 C and 10 C is also significantly better than that of other doped samples, showing excellent high rate performance. The specific capacities of LMCNO-0.08-0.06 samples at 5 C and 10 C are 94.9 mAh g^{-1} and 85.6 mAh g^{-1}, respectively. After 1000 charge discharge cycles, their capacity retention rates are 73.55% and 67.29%, respectively, showing a good diffusion rate of Li^+.

3.4. Cyclic Volt Ampere (CV) Test

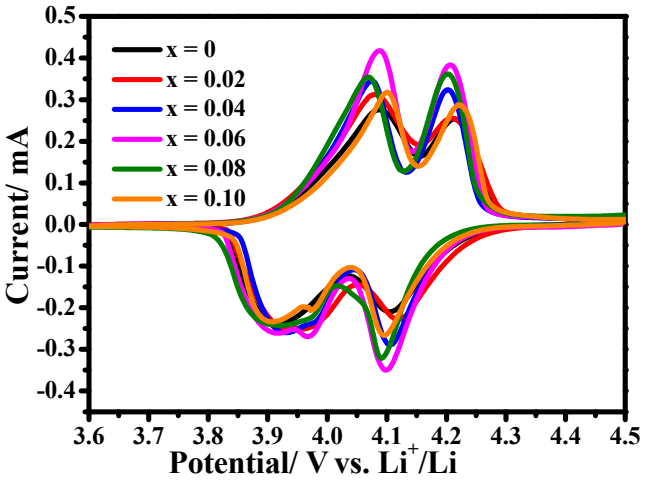

Figure 4. CV Curve of $LiMn_{1.92-x}Cu_{0.08}Ni_xO_4$

Figure 4 shows the CV curve of LiMn(11)Cu(12)Ni(13)O(14)($0 \leq x \leq 0.1$) sample. It can be seen from the figure that all CV curves show two pairs of obvious redox peaks near 3.95/4.05 V and 4.10/4.20 V, which is represented by the two-step de embedding process(137)of Li(81)in the bulk phase. This phenomenon corresponds to the first charge discharge plaorm in Figure 3b. It can be seen from Figure 4 that LMCNO-0.08-0.06 sample shows relatively large peak current and peak area, which means that it has small electrode polarization and excellent electrochemical reversibility.

3.5. AC impedance (EIS) test

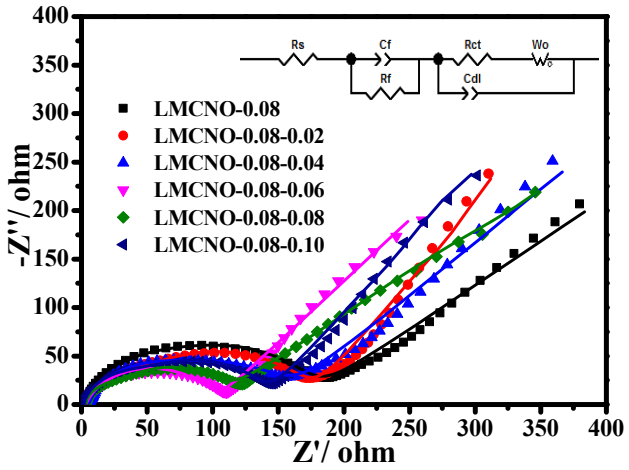

Figure 5. Nyquist Curve of $LiMn_{1.92-x}Cu_{0.08}Ni_xO_4$

Figure 5 shows the Nyquist diagram obtained by $LiMn_{1.92-x}Cu_{0.08}Ni_xO_4$ sample at room temperature. It can be seen from the diagram that all Nyquist curves are composed of a flat semicircle formed by overlapping two semicircles from high frequency region to medium frequency region and a diagonal line in low frequency region. The illustration is an equivalent analog circuit. The semicircle in the high and intermediate frequency region represents the charge transfer resistance (R_{ct}), and its formation is related to the double-layer capacitance (C_{dl}) [25, 26]; The distance from the horizontal axis intersection to the origin represents the solution resistance/ohmic resistance (R_s) [27, 28]; The semicircle in the intermediate frequency region can be attributed to the migration resistance (R_f of Li^+ through the multilayer surface film, and its formation is related to the limiting capacitance (C_f of the film thickness effect [29]; The diagonal area represents Warburg impedance (W_0), reflecting the diffusion process of Li^+ [30]. Fitting the Nyquist curve of the sample according to its equivalent

circuit diagram shows that when the Ni doping amount x=0, 0.02, 0.04, 0.06, 0.08 and 0.10, the corresponding R_{ct} values are 163.2, 150.2, 131.8, 97.55, 104.78 and 158.1 Ω, respectively. The R_{ct} value decreases first and then increases with the increase of the Ni doping amount, and is the smallest when x=0.06, that is, LMCNO-0.08-0.06 sample has the best reaction kinetics performance.

4. CONCLUSIONS AND OUTLOOK

In this paper, spinel $LiMn_{1.92-x}Cu_{0.08}Ni_xO_4$ ($0 \le x \le 0.1$) cathode materials were successfully prepared by solution combustion method. XRD and SEM data analysis results show that Ni^{2+} doping does not change the initial spinel structure, and with the increase of Ni^{2+} doping amount, the particle size gradually decreases, the polyhedron contour gradually appears, and the crystallinity tends to increase. The constant current charge discharge test results show that the doping of Ni^{2+} effectively improves the cycle stability and rate performance of the materials. $LiMn_{1.86}Cu_{0.08}Ni_{0.06}O_4$ samples show an initial discharge specific capacity of 103.4 mAh g^{-1} at room temperature of 1 C. After 1000 charge discharge cycles, the capacity retention rate is also as high as 67.80%. At high current densities of 5 C and 10 C, 94.9 mAh g^{-1} and 85.6 mAh g^{-1} of high initial discharge specific capacity were also released, respectively. After 1000 cycles, the capacity retention rates were 73.55% and 67.29%, respectively, showing a good diffusion rate of Li^+. CV test and EIS test also further proved that $LiMn_{1.86}Cu_{0.08}Ni_{0.06}O_4$ electrode has small polarization and excellent electrochemical reversibility, showing the smallest charge transfer resistance of 97.55 Ω.

REFERENCES

[1] Li Yan, Lu Yao, Guo Junming, etc Research progress of lanthanum modified spinel $LiMn_2O_4$ cathode material [J] Battery, 2020, 50 (01): 78-82.

[2] Chen Shoubin, Wu Xianming, Chen Shang, etc Study on $LiAlO_2$ coated spinel $LiMn_2O_4$ and its electrochemical properties [J] Modern Chemical Industry, 2016, 36 (04): 68-71.

[3] Yao Yuanlu, Li Guicun Preparation and electrochemical properties of high energy density $LiMn_2O_4$ microspheres [J] Journal of Qingdao University of Science and Technology: Natural Science Edition, 2014, 1, 18-23.

[4] Zhao Anting, Zhang Chaoping Synthesis and electrochemical properties of $LiCr_{0.05}Ni_{0.15}Mn_{1.8}O_4$ [J] Non ferrous metals, 2008, 4, 32-36.

[5] Hu Guojin, Ouyang Chuying The influence of surface effect on the performance of $LiMn_2O_4$ cathode material for lithium ion batteries [J] Journal of Physics, 2010, 8, 696-702.

[6] Liu Qilin, Hu Qishan Preparation and properties of $LiMn_{1.95}Mg_{0.05}O_{3.9}F_{0.1}$ as cathode material for lithium ion batteries [J] New Chemical Materials, 2016, 044 (012): 170-173.

[7] Capsoni D, Bini M, Chiodelli G, et al. Inhibition of Jahn-Teller cooperative distortion in $LiMn_2O_4$ spinel by Ga^{3+} doping [J]. Physical Chemistry Chemical Physics, 2002, 3(11):2162-2166.

[8] Kyung Y C, Chabg W R, Kwang B K. Onset Mechanism of Jahn-Teller Distortion in 4 V $LiMn_2O_4$ and Its Suppression by $LiM_{0.05}Mn_{1.95}O_4$ (M = Co, Ni) Coating [J]. Journal of the Electrochemical Society, 2005, 152(4):A791-A795.

[9] Mu Deying, Liu Yuanlong, Dai Changsong Research progress of liquid organic electrolyte for lithium ion battery [J] Battery, 2019, 49 (01): 68-71.

[10] Yang Zhanxu, Qiao Qingdong, Kang Xiaoxue Recent research progress of spinel $LiMn_2O_4$ cathode material [J] Modern Chemical Industry, 2012, 32 (01): 14-18.

[11] Wen Bixia, Tian Liang, Su Changwei, etc Research progress in microwave synthesis of spinel lithium manganate cathode materials [J] Battery, 2019, 49 (04): 342-345.

[12] Nie Wei, Liu Xiaolin, Wu Hai, etc Effect of alkaline earth metal ions on the properties of $LiNi_{0.5}Mn_{1.5}O_4$ [J] Battery, 2019, 49 (04): 278-282.

[13] Iqbal A. Effect of Ni and Cu Substitution on the Crystal Structure, Morphology and Electrochemical Performance of Spinel $LiMn_2O_4$ [J]. Int. J. Electrochem. Sci., 2019, 14, 929-942.

[14] You Meiling, Huang Xingkang, Tong Qingsong Study on the preparation and electrochemical properties of spinel $LiCo_{1+x}Mn_{1-x}O_4$ (x=0, 0.05, 0.1) materials [J] Guangzhou Chemical Industry, 2013, 12, 109-111.

[15] Xu Ning, Liu Guoqiang, Zeng Chaochao, etc Electrochemical properties of spinel $LiNi_xMn_{2-x}O_4$ lithium ion cathode material [J]. Chinese Journal of Nonferrous Metals, 2003, 1, 81-84.

[16] Chen Meng, Song Xiaona, Yang Chuang Synthesis and properties of doped spinel $LiAl_xMn_{2-x}O_4$ [J] Applied Science and Technology, 2005, 11, 60-62.

[17] Shu J, Yi T F, Shui M, et al. Comparison of electronic property and structural stability of $LiMn_2O_4$ and $LiNi_{0.5}Mn_{1.5}O_4$ as cathode materials for lithium-ion batteries [J]. Computational Materials Science, 2010, 50(2):776–779.

[18] Duan Y Z, Guo J M, Xiang M W, et al. Single crystalline polyhedral $LiNi_xMn_{2-x}O_4$ as high-performance cathodes for ultralong cycling lithium-ion batteries [J]. Solid State Ionics, 2018, 326, 100-109.

[19] Zhang Na, Tang Zhiyuan, Lu Xinghe Synthesis and properties of binary doped spinel $LiMn_2O_4$ [J] Modern Chemical Industry, 2005, 25 (1): 201-203.

[20] Peng C, Huang J, Guo Y, et al. Electrochemical performance of spinel $LiAl_xMn_{2-x}O_4$ prepared rapidly by glucose-assisted solid state combustion synthesis [J]. Vacuum, 2015, 120, 121-126.

[21] Zhao Anting, Zhang Chaoping Synthesis and electrochemical properties of $LiCr_{0.05}Ni_{0.15}Mn_{1.8}O_4$ [J] Nonferrous Metal Engineering, 2008, 60 (004): 30-34.

[22] Yu Yue, Bai Hongli, Liu Xiaofang, etc $LiNi_xMn_{2-x}O_4$ ($x \leq 0.10$) was synthesized by liquid phase flameless combustion and its electrochemical properties were studied Battery Industry, 2018123 (02): 62-69.

[23] Jiang Cuina, Li Hong, Luo Yutao, etc Experimental study on the influence of temperature and discharge rate on battery performance [J] Science, Technology and Engineering, 2013, 13 (009): 2496-2502.

[24] Deng Y, Mou J, Wu H, et al. A superior Li_2SiO_3 composited $LiNi_{0.5}Mn_{1.5}O_4$ cathode for high-voltage and high-performance lithium-ion batteries [J]. Electrochim Acta, 2017, 235, 19-31.

[25] Xiao Zhuobing Interface process of lithium ion in $LiMn_2O_4$ cathode material [J] Journal of Jishou University (Self Science Edition), 2004, 4, 53-57.

[26] Zhao S X, Fan X F, Deng Y F, et al. Structure and electrochemical performance of single-crystal $Li_{1.05}Ni_{0.1}Mn_{1.9}O_{3.98}F_{0.02}$ coated by Li–La–Ti–O solid electrolyte [J]. Electrochimica Acta, 2012, 65, 7-12.

[27] Zheng Zishan, Tang Zilong Studies on the Structural Characteristics and Electrochemical Properties of $Li_{1+x}Ni_yMn_{2-x-y}O_4$ Materials [J] Journal of Silicate, 2002, 30 (4): 456-459.

[28] Xiang M W, Su C W, Feng L L, et al. Rapid synthesis of high-cycling performance $LiMg_xMn_{2-x}O_4$ ($x \leq 0.20$) cathode materials by a low-temperature solid-state combustion method [J]. Electrochimica Acta. 2014, 125, 524-529.

[29] Duan Yuzhen, Zhu Jinyu, Guo Junming, et al. Synthesis and electrochemical properties of spinel lithium manganate cathode material $LiNi_{0.01}Co_{0.03}Mn_{1.96}O_4$ [J] Journal of Chemistry of Universities, 2019, 40 (12): 2574-2582.

[30] Chen Huan, Shan Shentao, Shen Chaoqi, etc One step synthesis of spinel lithium manganate by dynamic hydrothermal method and its properties [J]. Journal of Zhejiang University of Technology, 2019, 47 (05): 513-519.